FRONTIERS OF PHYSICS

RESEARCH ARTICLE
Volume 18 / Issue 1 / 13302 / 2023

Magnetic properties and critical behavior of quasi-2D layered Cr_4Te_5 thin film

Hao Liu[1,2], Jiyu Fan[1,2,†], Huan Zheng[1,2], Jing Wang[1,2], Chunlan Ma[3], Haiyan Wang[4], Lei Zhang[5], Caixia Wang[6], Yan Zhu[1,2], Hao Yang[1,2,‡]

1 Department of Applied Physics, College of Physics, Nanjing University of Aeronautics and Astronautics, Nanjing 211106, China
2 Key Laboratory of Aerospace Information Materials and Physics (NUAA), MIIT, Nanjing 211106, China
3 Jiangsu Key Laboratory of Micro and Nano Heat Fluid Flow Technology and Energy Application, School of Mathematics and Physics, Suzhou University of Science and Technology, Suzhou 215009, China
4 School of Materials Engineering, Purdue University, West Lafayette, IN 47907, USA
5 High Magnetic Field Laboratory, Chinese Academy of Sciences, Hefei 230031, China
6 College of Physics Science and Technology, Yangzhou University, Yangzhou 225002, China
Corresponding authors. E-mail: †jiyufan@nuaa.edu.cn, ‡yanghao@nuaa.edu.cn
Received June 25, 2022; accepted October 3, 2022

ABSTRACT

Quasi-2D layered Cr_4Te_5 thin film has attracted great attention because it possesses the high Curie temperature close to room temperature and relatively large saturation magnetization. However, the magnetic interactions and the nature of magnetic phase transition in the Cr_4Te_5 film have not been explored thoroughly. In this paper, we focused on the critical behavior of its magnetic phase transition through the epitaxial Cr_4Te_5 film fabricated by pulsed laser deposition (PLD). The final critical exponents $\beta = 0.359(2)$ and $\gamma = 1.54(2)$ were obtained by linear extrapolation together with Arrott-Noakes equation of state, and their accuracy was confirmed by using the Widom scaling relation and scaling hypothesis. We find that some magnetic disorders exist in the Cr_4Te_5 film system, which is related to Cr_4Te_5 critical behavior why its critical behavior is quite far from any conventional universality class. Furthermore, we also determined that the Cr_4Te_5 film exhibits a quasi-2D long-range magnetic interaction. Finally, the itinerant ferromagnets of Cr_4Te_5 films were confirmed by the Takahashi's self-consistent renormalization theory of spin fluctuations. Our work provides a new idea for understanding the mechanism of magnetic interactions in similar 2D layered films.

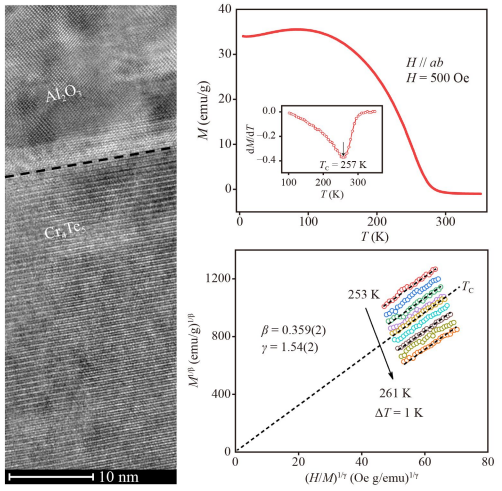

1 Introduction

Two-dimensional (2D) materials are in the spotlight owing to their peculiar optical, electrical, magnetic, and mechanical properties since the exfoliation of single-layer graphene from graphite [1–4]. Among them, 2D magnetic materials have become one of the recent focuses of research in material and physics science because of their potential applications in spintronics devices, data storage, and so on [5–8]. It has long been assumed that 2D materials are often not magnetic because thermal fluctuations destroy the long-range magnetic order of 2D systems according to the Mermin –Wagner theorem [9]. Therefore, researchers

Higher Education Press

https://doi.org/10.1007/s11467-022-1210-1

have attempted to introduce magnetism to 2D materials using defects and doping in the earlier study [10–12]. However, these materials are merely weak magnetic and exhibit short-range magnetic order, which limits the application prospects of these materials. Long-range magnetic orders are found in the CrI_3 and $Cr_2Ge_2Te_6$ systems until 2017 [13, 14], marking the research of 2D magnetic materials reaching a new stage. Studies have demonstrated that these materials exhibit long-range magnetic order because magnetic anisotropy has overcome thermal fluctuations [13].

Researchers have been searching for new 2D magnetic materials that display both high Curie temperature (T_C) and superior ferromagnetism properties. Although some 2D magnetic materials with long-range magnetic order have been found in the earlier study, their T_C is still very low, such as CrI_3 ($T_C = 61$ K) and $Cr_2Ge_2Te_6$ ($T_C = 66$ K) [15, 16]. Until very recently, both theoretical calculation and experimental results demonstrated that layered Cr_xTe_y compounds are excellent 2D magnetic materials [17–20]. In recent years, there are a lot of reports about Cr_xTe_y compounds. Multiple studies have found that monolayer $CrTe_2$ crystal is antiferromagnetic [21, 22], while $CrTe_2$ multilayers are ferromagnetic [23, 24], demonstrating the intricacy of 2D magnetic materials. Both monolayer and multilayers Cr_2Te_3 are ferromagnetic, and the monolayer Cr_2Te_3 has a T_C close to room temperature, while the Cr_2Te_3 multilayers T_C decreases significantly with the increase of thickness, which indicates that Cr_2Te_3 is a ferromagnetic materials regulated by thickness [25–27]. Moreover, there are many studies of $CrTe_3$-$CrTe_2$ heterojunctions. The $CrTe_3$-$CrTe_2$ heterojunctions fabricated by Yao *et al.* [28] exhibits rich magnetic properties and high tunability, which might allow multiple operation modes for future miniaturized spintronic devices. Li *et al.* [29] constructed $CrTe_3$-$CrTe_2$ planar heterojunctions and achieved a controllable phase transition from $CrTe_3$ into $CrTe_2$ via vacuum annealing, which provides a possibility of fabricating highly integrated magnetic tunnelling junctions by local heating of the $CrTe_3$ films. In addition to possessing a higher saturation magnetization, Cr_xTe_y compounds also have T_C close to or higher than room temperature. Among them, quasi-2D Cr_4Te_5 single crystal has T_C up to 322 K and a saturation magnetization of approximately 70 emu/g [20]. Our prior studies found that epitaxial films of Cr_4Te_5 still possess the T_C close to room temperature and relatively high saturation magnetization [30, 31]. Therefore, this film has many potential applications, such as spintronic devices.

This study successfully fabricated the epitaxial Cr_4Te_5 film and investigated its microstructure and magnetic properties in detail. To better understand the magnetic interactions and the magnetic phase transition of Cr_4Te_5 film and to understand why it has nearly room-temperature ferromagnetism, we also carefully investigated the phase transition and critical behavior of this film.

2 Experimental details

We prepared the single-crystalline Cr_4Te_5 films by pulsed laser deposition (PLD) on (006)-oriented Al_2O_3 substrates. Before experiments, the Al_2O_3 substrates were sequentially cleaned with deionized distilled water, acetone and ethanol by ultrasonication. The substrate temperature of 550 °C, the chamber vacuum level of 10^{-4} Pa, the KrF excimer laser ($\lambda = 248$ nm) energy density of 1.8 J/cm^2 and the laser repetition rate of 4 Hz were maintained during Cr_4Te_5 film depositions. Both out-of-plane θ-2θ scan and in-plane ϕ-scan were performed by using high-resolution X-ray diffraction (XRD, Panalytical) to characterize the growth quality and crystal structure of the films. The microstructure, thicknesses and the elemental mappings of the samples were observed using Scanning Transmission Electron Microscope (STEM, FEI talos F200X). The surface morphology of Cr_4Te_5 thin films were characterized by Atomic Force Microscopy (AFM, Asylum Research). The magnetic properties of the films were measured by means of a Magnetic Properties Measurement System (MPMS, Quantum Design), and the diamagnetic contributions of the Al_2O_3 substrate and sample holder have been subtracte from magnetic data.

3 Results and discussion

Figure 1(a) presents the XRD θ–2θ diffraction pattern of Cr_4Te_5 film on an Al_2O_3 substrate. In addition to the (006) peak of the Al_2O_3 substrate, only (00l) peaks of the Cr_4Te_5 film are observed in Fig. 1(a), suggesting that the films are highly c-axis oriented. XRD in-plane ϕ-scan patterns of Cr_4Te_5 (222) and Al_2O_3 (104) were graphically illustrated in Fig. 1(b). The ϕ-scan of the film has six peaks spaced 60 degrees apart, indicating that the Cr_4Te_5 film (222) plane is a six-axis symmetric structure, and the films are highly in-plane oriented. The combined results of out-of-plane and in-plane indicate that the Cr_4Te_5 film is epitaxial grown on the Al_2O_3 substrate. The cross-section TEM image in Fig. 2(a) reveals that the thickness of the Cr_4Te_5 film is approximately 125 nm. Figure 2(b) exhibits the high-resolution TEM image of Cr_4Te_5 and Al_2O_3 interface. Clearly, the Cr_4Te_5 films grow in 2D layer-by-layer mode parallel to the interface. In addition, Fig. S1(a) shows the locally magnified high-resolution TEM image of Cr_4Te_5, and (b) presents the schematic diagram of the crystal structure of Cr_4Te_5. Figure 2(c) presents the general surface morphology of the 125 nm-thick Cr_4Te_5 film measured with AFM, and the average surface roughness of the film is 3.08 nm. Furthermore, it can also be observed that the surface morphology of this film was relatively

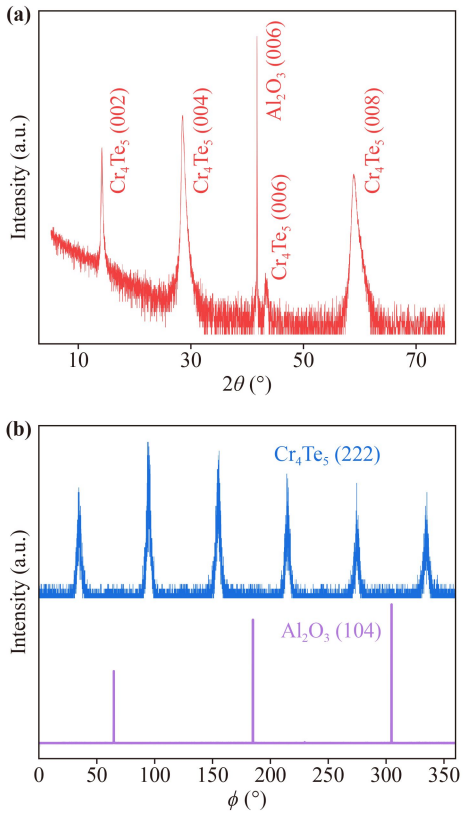

Fig. 1 **(a)** XRD θ–2θ pattern of Cr_4Te_5 film grown on Al_2O_3 substrate. **(b)** XRD ϕ-scan pattern of Cr_4Te_5 (222) and Al_2O_3 (104).

homogeneous and flat. Figure 2(d) shows the topographic height profile taken along the red line of Fig. 2(c). The maximum height difference film surfaces is approximately 7 nm, suggesting that the film surface is relatively flat and smooth. Moreover, Fig. 3 shows the High-angle annular dark-field (HAADF) STEM image of the Cr_4Te_5 /Al_2O_3 sample, and corresponding energy-dispersive spectroscopy (EDS) mappings of Cr, Te, Al and O elements. Figures 3(d) and (e) confirm the presence of Al and O elements in the Cr_4Te_5 thin films, which is consistent with prior reports of Cr_2Te_3 thin films by Li *et al.* [25]. They suggested that the Al was sourced from the diffusion of the Al_2O_3 substrate, and O was sourced from external environment and the diffusion of the substrate. Further, they also demonstrate that Al doping has distinct regulatory effects on magnetic properties of Cr_2Te_3 films, but the O element has a negligible effect.

The temperature dependence of magnetization, $M(T)$, from 5–350 K for Cr_4Te_5 film samples measured under an external magnetic field of 500 Oe is shown in Fig. 4 (a). A magnetic transition from the low-temperature FM to high-temperature PM state is observed during the heating process. One of the ferromagnetic materials' most important physical properties is the T_C, i.e., FM–PM phase transition temperature. As shown in the left inset of Fig. 4(a), the minimum determines the T_C = 257 K in the dM/dT vs. T curve. This value is slightly smaller than those of the Single-crystalline Cr_4Te_5 samples (T_C = 322 K) [20], but consistent with previous reports for Cr_4Te_5 films [30, 31]. Decreased T_C of thin films may be associated with thickness variation effect; that is, the thickness of the film is much less than a single crystal since many studies demonstrate that the T_C of a 2D magnetic material drops severely when the thickness is reduced to a monolayer or few layered [31, 32]. The right inset of Fig. 4(a) shows the magnetic hysteresis loops of the Cr_4Te_5 films at 5 K and the saturation magnetic moment reaches ~ 40 emu/g. In order to investigate the magnetic properties and the critical behaviors of the Cr_4Te_5 films and, in turn, to clarify the nature of FM-PM phase transition, we have measured the initial isothermal magnetization curves in the vicinity of T_C. Figure 4(b) depicts initial isothermal magnetization (M vs. H) curves measured at different temperatures between 253 and 261 K in an interval of 1 K for Cr_4Te_5 films. As illustrated in Fig. 4(b), all M(H) curves rise sharply in the low-field region and increase slowly in the high-field region, which correspond to the behavior of ferromagnets.

In order to clarify the magnetic interactions and the nature of magnetic phase transition in the vicinity of T_C, critical behavior analysis was performed for Cr_4Te_5 film samples. According to the scaling hypothesis [33, 34], the critical behavior of the magnetic phase transition materials in the vicinity of T_C can be characterized by the critical exponents β, γ and δ. These critical exponents β (associated with the spontaneous magnetization M_S below T_C), γ (associated with the initial inverse magnetic susceptibility χ_0^{-1} above T_C) and δ (associated with the critical magnetization isotherm M at T_C) can be expressed by the following equations, respectively [33, 34]:

$$M_S(T) = M_0(-\varepsilon)^{\beta}, \varepsilon < 0,\ T < T_C, \tag{1}$$

$$\chi_0^{-1}(T) = (h_0/m_0)\,\varepsilon^{\gamma}, \varepsilon > 0,\ T > T_C, \tag{2}$$

$$M = DH^{1/\delta}, \varepsilon = 0,\ T = T_C. \tag{3}$$

In above equations, M_0, h_0/m_0 and D are the critical amplitudes in the above equations, and $\varepsilon = (T - T_C)/T_C$ is the reduced temperature. Moreover, when both β and γ were appropriate, the relationship between H/M and M in the vicinity of T_C follows the Arrott–Noakes equation of state [35]:

$$(H/M)^{1/\gamma} = A' + B'M^{1/\beta}, \tag{4}$$

where coefficients A' and B' are related to temperature. According to the abovementioned formula, in the modified Arrott plots [$M^{1/\beta}$ vs. $(H/M)^{1/\gamma}$, or Arrott plot], by choosing the appropriate values of β and γ, the curve of

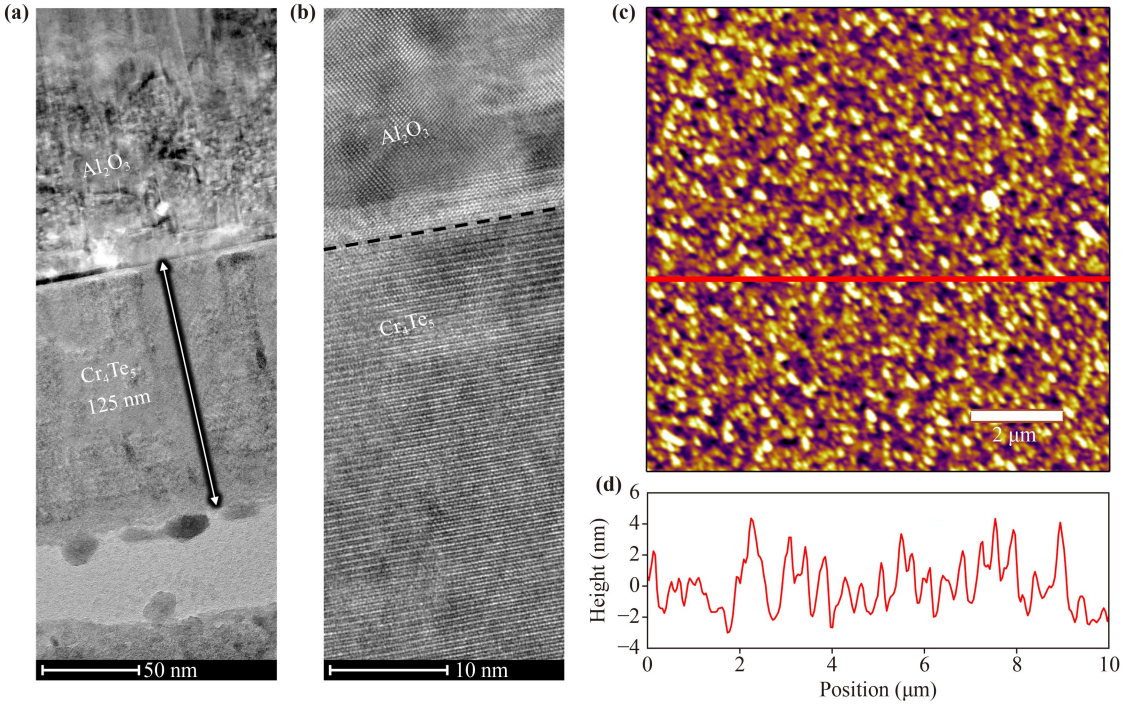

Fig. 2 **(a)** Cross-sectional TEM image and **(b)** high-resolution TEM image of Cr_4Te_5 and Al_2O_3 interface. **(c)** AFM topographic image of Cr_4Te_5 film surface. **(d)** Height profile obtained along the red line in (c).

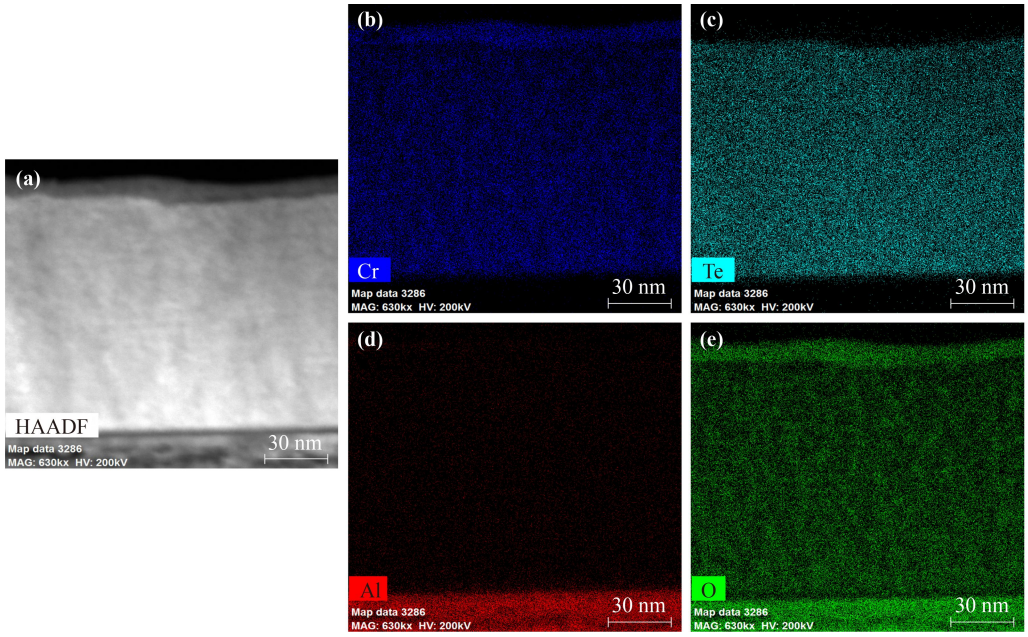

Fig. 3 **(a)** HAADF-STEM image of Cr_4Te_5 and Al_2O_3 interface. **(b–e)** EDS mapping of Cr, Te, Al, and O element, respectively.

T_C should pass the origin and all curves should form a series of parallel lines in the high field region.

Figure 5(a) represents the Arrott plot ($\beta = 0.5$ and $\gamma = 1$) based on Landau mean-field model [35]. Clearly, all the slope of all the curves in the Arrott plot are positive. So, according to the Banerjee criterion [36], the phase transition in the Cr_4Te_5 film has a second-order nature. Unfortunately, the curve of T_C is not a straight line through the origin, indicating that the Landau mean-field theory does not apply to explain the magnetic interactions and the critical behavior of the Cr_4Te_5 film by according to Arrott–Noakes equation of state [37]. Furthermore, Fig. S2 shows the Modified Arrott plots based on four most common theoretical models, which are 3D-Heisenberg, 3D-Ising, 3D-XY and Tricritical mean field model, respectively. The curve of T_C in all

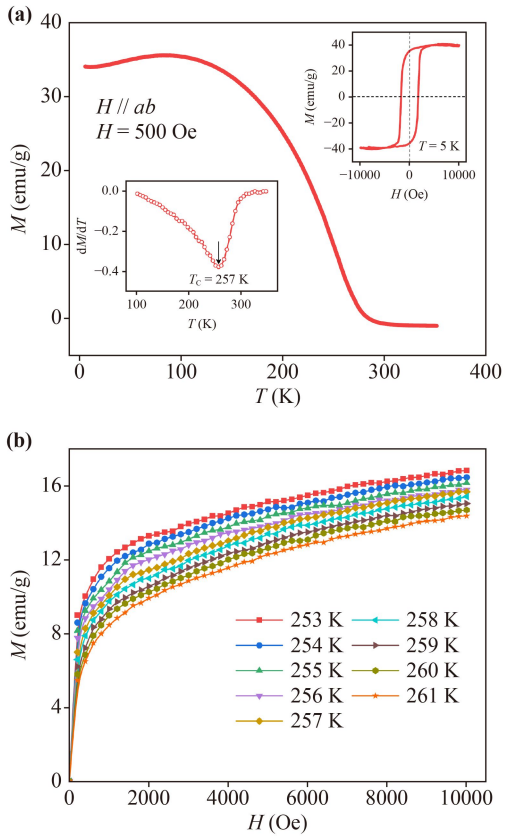

Fig. 4 **(a)** Temperature dependence of magnetization under 500 Oe applied magnetic field for Cr_4Te_5 film samples. Left inset: The dM/dT vs. T curve. Right inset: The hysteresis loops for 5 K. **(b)** Typical initial isothermal magnetization curves measured around T_C.

models are a straight line pass through the origin, as illustrated in Fig. S2. However, it is clear that all the curves of the four models are not perfectly parallel in the high field region. This also shows that these four common theoretical models are not suitable for explaining the critical behavior and magnetic interactions of the Cr_4Te_5 film. Although none of the four theoretical models are very suitable, choosing a relatively good one for further research is still necessary. So, the normalized slopes [$NS = S(T)/S(T_C)$, where $S(T)$ is the slope of the curve with temperature T in the modified Arrott plots] were calculated. The magnetic field range for calculating $S(T)$ is from 3000 to 10000 Oe. According to the Arrott–Noakes equation of state [37], all curves should form a series of parallel lines in the high field region of the modified Arrott plot. That is, the value of NS should be equal to one. Figure 5(b) shows the NS as a function of temperature for the four common theoretical models mentioned above. Indeed, there is not much difference between 3D-Heisenberg, 3D-Ising and 3D-XY model, so we chose 3D-Heisenberg model for further studies.

In order to obtain the more accurate critical exponents and the critical temperature of the Cr_4Te_5 film system, the linear extrapolation was performed based on the modified Arrott plot of 3D-Heisenberg model. Based on Eqs. (1) and (2), using linear extrapolation and rigorous iterative method [37, 38], the values of the critical exponents for convergence were obtained. The final obtained critical exponents are $\beta = 0.359(2)$ with $T_C = 256.3(7)$ K and $\gamma = 1.54(2)$ with $T_C = 256.9(5)$ K. Figure 5(c) shows the temperature dependence of M_S (left axis) and χ_0^{-1} (right axis) obtained from the last time linear extrapolation and the red solid line is the fitting curves by using Eqs. (1) and (2). The final critical exponents obtained by rigorous iterative method are far from the critical exponents of 3D-Heisenberg model ($\beta = 0.365$, $\gamma = 1.386$). This is reasonable because of the critical exponents do not depend on the initial parameters. The values of T_C obtained from the fitting of $M_S(T)$ and $\chi_0^{-1}(T)$ curves are close to the value obtained from dM/dT versus T curve. Figure 5(d) depicts the final Modified Arrott plot constructed using the final critical exponents $\beta = 0.359(2)$ and $\gamma = 1.54(2)$. It clear that the linear extrapolation (the black dashed line) of T_C curve from the high field region in Fig. 5(d) passes through the origin, on the other hand, all curves form a series of parallel lines in the high field. These results were all consistent with the requirements of the Arrott–Noakes equation of state. Furthermore, the values of temperature coefficients A' and B' in the Eq. (4) are obtained by fitting the data in the final modified Arrott plot. Figure 6(a) shows the obtained coefficients A' and B' change with temperature. Obviously, coefficient B' reaches its minimum at T_C and the value of coefficient A' is equal to zero at T_C. This further indicates the value of the critical exponents fulfil the requirements of the Arrott-Noakes equation [39, 40].

The value of the third critical exponent δ can be obtained by fitting the initial isothermal magnetization $M(H)$ curve at T_C, as defined by Eq. (3). Figure 6(b) presents the M versus H curve at $T_C = 257$ K and the inset shows the same curve on the log-log scale, and the black solid line is the fit following the Eq. (3). The value of the third critical exponent δ obtained from fitting is $\delta = 5.24(1)$. Furthermore, the value of δ also can be obtained by the Widom scaling relation [41, 42]:

$$\delta = 1 + \frac{\gamma}{\beta}. \tag{5}$$

The values of critical exponents $\beta = 0.359(2)$ and $\gamma = 1.54(2)$ are from the final Modified Arrott plot. After the calculation, the value of the third critical exponent δ is 5.29(3), which is consistent with the value $\delta = 5.24(1)$ from fitting M versus H curve. This also confirms that the the final obtained critical exponents β and γ are unambiguous and consistent.

In addition, the reliability of the critical exponents β and γ obtained from the linear extrapolation can also be assessed using the scaling hypothesis [34, 43]. According to the scaling equation of state, the relationship of the

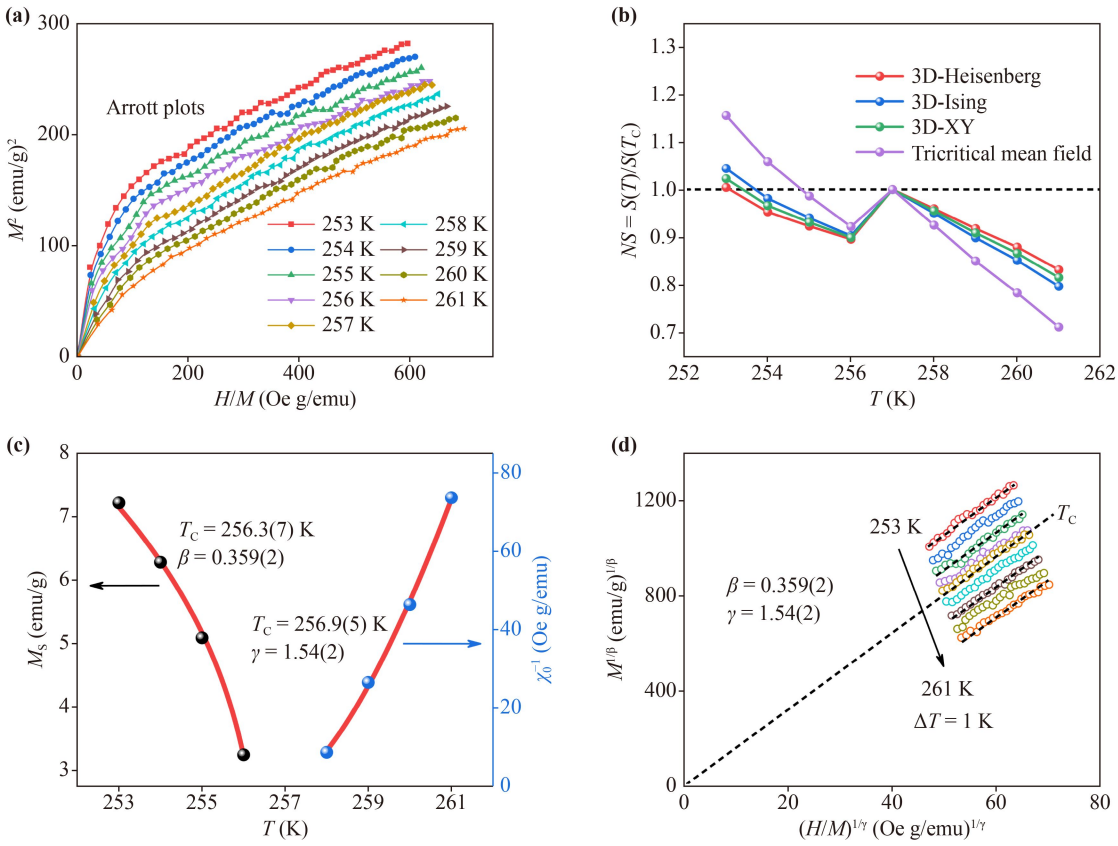

Fig. 5 **(a)** The Arrott plot of M^2 vs. H/M. **(b)** Normalized slope (NS) of four common theoretical models as a function of temperature. **(c)** Temperature dependence of the spontaneous magnetization M_S (left axis) and initial inverse magnetic susceptibility χ_0^{-1} (right axis), and the red solid lines are the fitting curves by using Eqs. (1) and (2). **(d)** The final modified Arrott plot [$M^{1/\beta}$ vs. $(H/M)^{1/\gamma}$] at the high-field region with the critical exponents $\beta = 0.359(2)$ and $\gamma = 1.54(2)$.

three variables M, H and T can be expressed as follows [34]:

$$M(H,\varepsilon) = \varepsilon^{\beta} f_{\pm}\left(\frac{H}{\varepsilon^{\beta+\gamma}}\right), \tag{6}$$

where $f_{\pm}$ (f_+ and f_-) are regular functions for $T > T_C$ and $T < T_C$, respectively. The renormalized magnetization is defined as $m \equiv \varepsilon^{-\beta} M(H,\varepsilon)$ and renormalized field is defined as $h \equiv \varepsilon^{-(\beta+\gamma)} H$ based on Eq. (6). If the critical exponents β and γ are appropriate, the plot of m versus h should correspond to two separate curves for the temperature above and below T_C, respectively. Figure 6(c) shows the plots of m versus h and the inset shows the same plot on a log–log scale. As shown in Fig. 6(c) and its inset, all $m(h)$ data collapse into two separate branches below and above T_C, respectively. This indicates that the critical exponents β and γ correspond to the scaling hypothesis. In all, either the Arrott-Noakes equation of state, Widom scaling relation, or scaling hypothesis indicates that the values of critical exponent β and γ are reliable and intrinsic. In other words, this critical exponents obtained in this study could be used to explain the magnetic interactions and the critical behavior of the Cr_4Te_5 film sample.

The obtained critical exponents $\beta = 0.359(2)$ and $\gamma = 1.54(2)$ did not conform to those mentioned above several common models indicating that the Cr_4Te_5 film system may have complex magnetic interactions. In order to obtain a deeper understanding of magnetic interactions in the Cr_4Te_5 film system, the effective critical exponents β_{eff} and γ_{eff} in the asymptotic region ($\varepsilon \to 0$) were calculated according to followed equations [44, 45]:

$$\beta_{eff} = \frac{d[\ln M_S(\varepsilon)]}{d(\ln \varepsilon)}, \gamma_{eff} = \frac{d[\ln \chi_0^{-1}(\varepsilon)]}{d(\ln \varepsilon)}. \tag{7}$$

Figure 6(d) presents how the effective critical exponents β_{eff} and γ_{eff} changes as the reduced temperature $-\varepsilon$ and ε changes. Obviously, in the asymptotic region, the effective critical exponents neither belong to any universality class nor are they close to the critical exponents [$\beta = 0.359(2)$ and $\gamma = 1.54(2)$] obtained by linear extrapolation. Because of the divergence of the correlation length in the vicinity of T_C, the critical exponents do not correlate with microscopic details of the magnetic system; that is, the static critical exponents obtained from linear extrapolation are universal properties, while the effective exponents are not [46, 47]. Moreover, β_{eff} is monotonic with $-\varepsilon$, but γ_{eff} is non-monotonic with ε. There have also

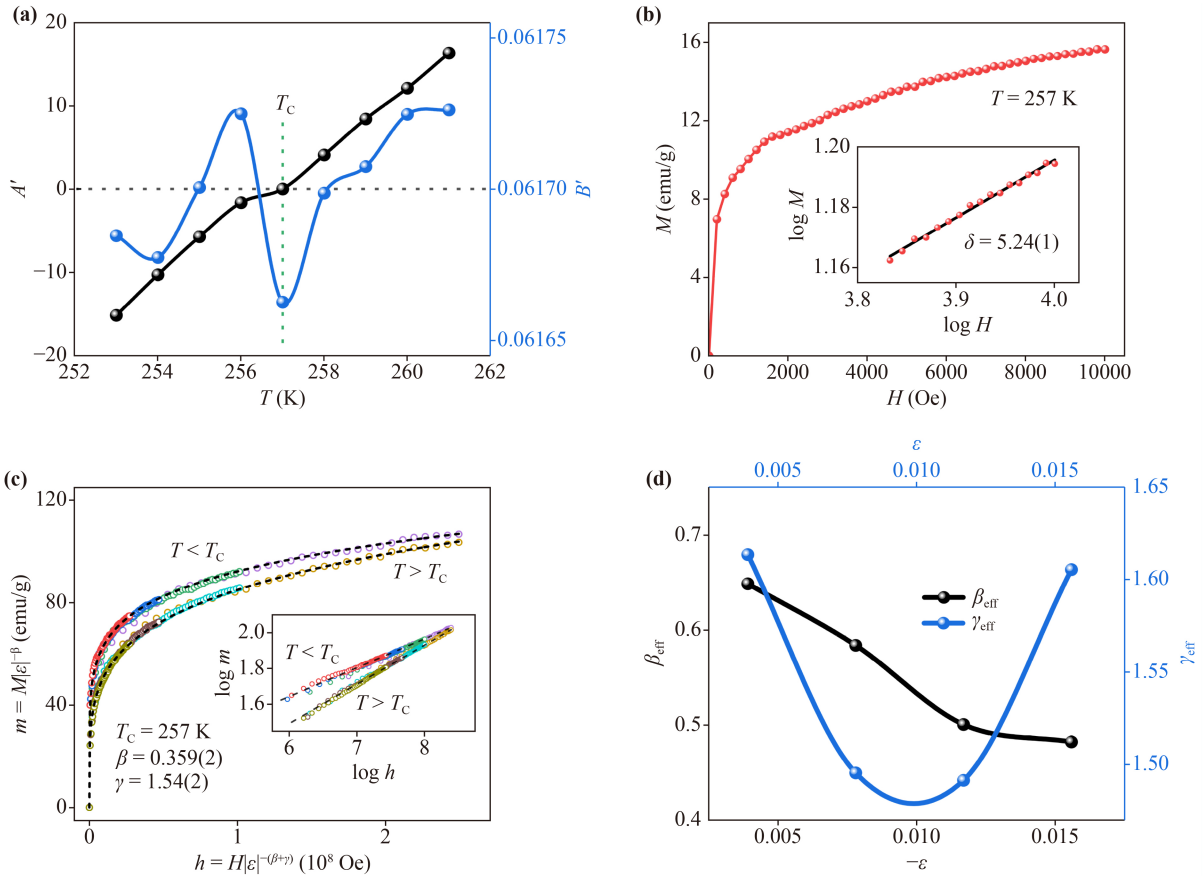

Fig. 6 **(a)** The coefficients A' and B' of the Arrott–Noakes equation as a function of temperature. **(b)** Initial isothermal magnetization curve at $T = 257$ K. Inset: The same curve on the log–log scale and the black solid line is the fit following Eq. (3). **(c)** $M(H)$ data are plotted as renormalized magnetization (m) vs. renormalized field (h) following scaling hypothesis. Inset: The same plot on the log–log scale. **(d)** Effective critical exponents β_{eff} and γ_{eff} as a function of the reduced temperature ε.

been many non-monotonic variations of effective critical exponents in some prior studies on critical behavior, often associated with systematic magnetic disorders [40, 48]. That is, some magnetic disorders may exist in the Cr_4Te_5 film system. Of course, the magnetic disorder contents in the film are minimal because the film has excellent ferromagnetic. Some defects are inevitably induced during film preparation, which may be why magnetic disorder exists. In addition, the Al element of substrate diffused into the film may also contribute to it. These might be the reason why the critical exponents eventually obtained do not conform to several common theoretical models. Of course, these may also be the reasons why the T_C of the thin film is much lower than that of the single-crystalline Cr_4Te_5 bulks.

Next, the nature and range of interactions were explored to better understand the complex magnetic interactions in this film. According to the renormalization-group theory analysis, in the long-range interaction, the interaction decays expression is $J(r) \approx r^{-(d+\sigma)}$, and in the short-range interaction, the expression is $J(r) \approx e^{-r/b}$, where r is the distance, d is the spatial dimensionality, σ is a positive constant and b is the spatial scaling factor [49]. Moreover, the value of σ determines whether the spin interaction is long-range or short-range. That is, $\sigma < 2$ corresponds to long-range interaction and $\sigma > 2$ corresponds to short-range interaction, respectively. The value of σ can be obtained from the relationship between σ and γ, as follows [50]:

$$\gamma = 1 + \frac{4}{d}\left(\frac{n+2}{n+8}\right)\Delta\sigma + \frac{8(n+2)(n-4)}{d^2(n+8)^2} \times \left[1 + \frac{2G\left(\frac{d}{2}\right)(7n+20)}{(n-4)(n+8)}\right]\Delta\sigma^2, \quad (8)$$

where n is the spin dimensionality, $\Delta\sigma = \sigma - \frac{d}{2}$ and $G\left(\frac{d}{2}\right) = 3 - \frac{1}{4}\left(\frac{d}{2}\right)^2$. The value of σ can be obtained by using Eq. (8), and the critical exponents can be further obtained by the σ and the following formula: $\nu = \gamma/\sigma$, $\alpha = 2 - \nu d$ and $\beta = (2 - \alpha - \gamma)/2$. According to $\gamma = 1.54(2)$, constant σ and all critical exponents for different sets of $\{d : n\}$ are calculated and listed in Table 1 for comparison. When $\{d : n\} = \{2 : 3\}$ and $\sigma = 1.3619$, $\beta = 0.3608$ and $\delta = 5.2683$ are obtained, as described in

Table 1 Comparison of critical exponents of Cr_4Te_5 films with different sets of $\{d : n\}$.

Critical exponents	$d = 3$	$d = 3$	$d = 3$	$d = 2$	$d = 2$	$d = 2$
	$n = 1$	$n = 2$	$n = 3$	$n = 1$	$n = 2$	$n = 3$
σ	2.2415	2.1286	2.0621	1.4736	1.4033	1.3619
α	–0.0611	–0.1705	–0.2404	–0.0902	–0.1948	–0.2616
β	0.2606	0.3152	0.3502	0.2751	0.3274	0.3608
δ	6.9105	5.8853	5.3976	6.5985	5.7039	5.2683

Table 1. These values most closely approximate those experimentally obtained critical exponents $\beta = 0.359(2)$ and $\delta = 5.24(1)$. So, the Cr_4Te_5 film corresponds to a long-range spin interaction system with $d = 2$ and $n = 3$, and the magnetic interaction decays as $J(r) \approx r^{-3.36}$.

The critical behavior of common 2D magnetic materials has been studied quite extensively. Earlier study has indicated that CrI_3 single crystal exhibits a 3D long-range magnetic coupling reported [16]. Later, the critical behavior analysis indicates that van der Waals (vdW) material Fe_3GeTe_2 and quasi-2D material $LaCrSb_3$ also exhibit 3D long-range magnetic coupling [51, 52]. A recent study of Cr_5Te_8 showed that its critical exponents are close to the 3D-Ising model [17]. However, Liu *et al.* [53] have shown that the magnetic coupling of $Cr_2Ge_2Te_6$ single crystal is of a 2D-Ising-like type. Similar result is also found in the study on quaternary vdW material $Cr_{0.96}Ge_{0.17}Si_{0.82}Te_3$ by Li *et al.* [54]. Moreover, it has been shown that vdW Fe_4GeTe_2 magnet exhibits a quasi-2D itinerant magnetism [55]. In summary, these studies suggest that the nature of magnetic properties in 2D single crystal magnetic materials may be 2D or 3D magnetic order.

Although the essences of magnetic properties in 2D single crystal are uncertain, it is noteworthy that the essence of magnetism changes as a function of thickness of 2D magnetic materials. The phase transition of a $CrCl_3$ single crystal is situated close to a 3D to 2D critical point [56]. However, the vdW $CrCl_3$ monolayer exhibits intrinsic 2D-XY ferromagnetism [57]. Similarly, single-crystalline CrI_3 follows the crossover critical behavior of mean-field model and 3D-Ising model [58]. Huang *et al.* [13] demonstrated that exfoliated monolayer CrI_3 exhibits a 2D ferromagnetism. Together, the essence of magnetic properties in these materials changes from 3D to 2D magnetic with decreasing thickness. Accordingly, it is reasonable that the spatial dimensionality of the spin system in Cr_4Te_5 single crystal is 3D while the Cr_4Te_5 film is 2D [20]. Taroni *et al.* [59] found the value of critical exponent β for 2D magnets range from 0.1 to 0.25. However, the value of β obtained in this study is outside the this range. Therefore, we think that the magnetic properties of Cr_4Te_5 film are quasi-2D in nature, which is similar to Fe_4GeTe_2 single crystal [55].

Finally, to elucidate the nature of ferromagnetism in the Cr_4Te_5 films, we analyzed its initial isothermal magnetization $M(H)$ curve at T_C using Takahashi's self-consistent renormalization (SCR) theory [55, 60, 61]. According to the SCR theory of spin fluctuations, the magnetization M and the magnetic field H at T_C should obey the following relation:

$$M^4 = \frac{1}{4.671}\left(\frac{T_C^2}{T_A^2}\right)\left(\frac{H}{M}\right), \tag{9}$$

where T_A is the dispersion of the spin fluctuation spectrum in wave-vector space. T_A, M and H are in units of K, μ_B/Cr and Oe, respectively. Figure 7 shows the M^4 versus H/M plot of the critical magnetization isotherm of the Cr_4Te_5 films. The M^4 shows a linear variation with H/M, as shown in the Fig. 7, which has been observed in some itinerant ferromagnetic compounds such as MnSi [62], Fe_4GeTe_2 [55] and $LaCo_2P_2$ [63]. Based on Eq. (9), $T_A = 1238$ K is obtained by linearly fitting the data presented in Fig. 7. According to the SCR theory, T_C can be described as

$$T_C = (60c)^{-3/4} P_S^{3/2} T_A^{3/4} T_0^{1/4} \quad (c = 0.3353), \tag{10}$$

where P_S is the spontaneous magnetization, and T_0 is the energy width of the dynamical spin fluctuation spectrum. P_S and T_0 are in units of μ_B/Cr and K, respectively. Using the values of $T_C = 257$ K, $P_S = 1.288$ μ_B/Cr, and $T_A = 1238$ K, we obtain the $T_0 = 4100$ K for Cr_4Te_5 films. According to the SCR theory of spin fluctuations, the ratio T_C/T_0 is an important parameter as it characterizes the degree of itineracy or localization of the spin moment [60, 61]. For $T_C/T_0 \ll 1$, magnetic materials exhibit itinerant magnetism, while for $T_C/T_0 \sim$

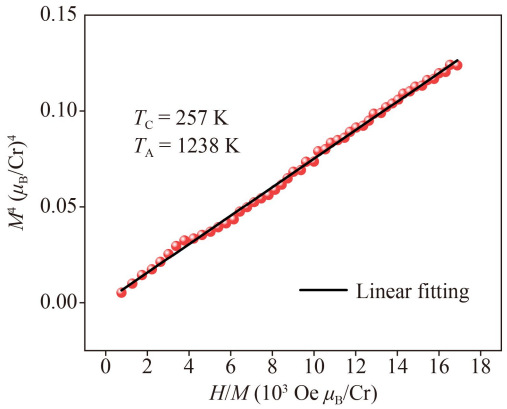

Fig. 7 The M^4 vs. H/M plot for the Cr_4Te_5 film at $T = 257$ K.

1, they exhibit localized magnetic moments. Here, for Cr_4Te_5 films, the ratio of T_C/T_0 is about 0.063, which suggests that the Cr_4Te_5 films should belong to itinerant ferromagnets.

4 Conclusion

In summary, we have fabricated the epitaxial Cr_4Te_5 film by PLD and investigated its growth quality, microstructure and magnetic properties in detail by XRD, TEM, AFM and PPMS. We studied the phase transition and critical behavior of this films near the $T_C = 257$ K. We determined the final critical exponents $\beta = 0.359(2)$ and $\gamma = 1.54(2)$ by linear extrapolation and confirmed their accuracy and reliability using the Arrott–Noakes equation of state, Widom scaling relation and scaling hypothesis, respectively. Furthermore, we found that some magnetic disorders may exist in the Cr_4Te_5 film system by calculating effective critical exponents, which may be the reason why the critical behavior of these films is quite far from any conventional universality class. We also determined that the Cr_4Te_5 film is quasi-2D long-range magnetic interactions and its magnetic interaction decays as $J(r) \approx r^{-3.36}$. Finally, we also demonstrate that the Cr_4Te_5 films are itinerant ferromagnets by using the Takahashi's self-consistent renormalization theory of spin fluctuations.

Electronic supplementary material Supplementary materials are available in the online version of this article at https://doi.org/10.1007/s11467-022-1210-1 and https://journal.hep.com.cn/fop/EN/10.1007/s11467-022-1210-1 and are accessible for authorized users.

Acknowledgements This work was supported by the National Natural Science Foundation of China (Grant Nos. 11974181, 12074386, and 11874358), the Postgraduate Research & Practice Innovation Program of Jiangsu Province (KYCX21_0177), the Top-notch Academic Programs Project of Jiangsu Higher Education Institutions (TAPP), and the Hongque Innovation Center (No. HQ202102003).

References

1. A. Hashimoto, K. Suenaga, A. Gloter, K. Urita, and S. Iijima, Direct evidence for atomic defects in graphene layers, *Nature* 430, 870 (2004)
2. Z.Lin, A. McCreary, N. Briggs, S. Subramanian, K. H. Zhang, Y. F. Sun, X. F. Li, N. J. Borys, H. T. Yuan, S. K. Fullerton-Shirey, A. Chernikov, H. Zhao, S. McDonnell, A. M. Lindenberg, K. Xiao, B. J. LeRoy, M. Drndic, J. C. M. Hwang, J. Park, M. Chhowalla, R. E. Schaak, A. Javey, M. C. Hersam, J. Robinson, and M. Terrones, 2D materials advances: From large scale synthesis and controlled heterostructures to improved characterization techniques, defects and applications, *2D Mater.* 3, 042001 (2016)
3. F. Bonaccorso, L. Colombo, G. H. Yu, M. Stoller, V. Tozzini, A. C. Ferrari, R. S. Ruoff, and V. Pellegrini, Graphene, related two-dimensional crystals, and hybrid systems for energy conversion and storage, *Science* 347, 1246501 (2015)
4. M. Gibertini, M. Koperski, A. F. Morpurgo, and K. S. Novoselov, Magnetic 2D materials and heterostructures, *Nat. Nanotechnol.* 14, 408 (2019)
5. H. Li, S. C. Ruan, and Y. J. Zeng, Intrinsic van Der Waals magnetic materials from bulk to the 2D limit: New frontiers of spintronics, *Adv. Mater.* 31, 1900065 (2019)
6. S. Rahman, J. F. Torres, A. R. Khan, and Y. R. Lu, Recent developments in van der Waals antiferromagnetic 2D materials: Synthesis, characterization, and device implementation, *ACS Nano* 15, 17175 (2021)
7. C. M. Acosta, E. Ogoshi, J. A. Souza, and G. M. Dalpian, Machine learning study of the magnetic ordering in 2D materials, *ACS Appl. Mater. Interfaces* 17, 9418 (2022)
8. L. S. Zhang, J. Zhou, H. Li, L. Shen, and Y. P. Feng, Recent progress and challenges in magnetic tunnel junctions with 2D materials for spintronic applications, *Appl. Phys. Rev.* 8, 021308 (2021)
9. N. D. Mermin, and H. Wagner, Absence of ferromagnetism or antiferromagnetism in one- or two-dimensional isotropic Heisenberg models, *Phys. Rev. Lett.* 17, 1133 (1966)
10. A. M. Hu, L. L. Wang, W. Z. Xiao, G. Xiao, and Q. Y. Rong, Electronic structures and magnetic properties in nonmetallic element substituted MoS_2 monolayer, *Comput. Mater. Sci.* 107, 72 (2015)
11. C. Ataca and S. Ciraci, Functionalization of single-layer MoS_2 honeycomb structures, *J. Phys. Chem. C* 115, 13303 (2011)
12. J. Zhang, J. M. Soon, K. P. Loh, J. H. Yin, J. Ding, M. B. Sullivian, and P. Wu, Magnetic molybdenum disulfide nanosheet films, *Nano Lett.* 7, 2370 (2007)
13. B. Huang, G. Clark, E. Navarro-Moratalla, D. R. Klein, R. Cheng, K. L. Seyler, D. Zhong, E. Schmidgall, M. A. McGuire, D. H. Cobden, W. Yao, D. Xiao, P. Jarillo-Herrero, and X. D. Xu, Layer-dependent ferromagnetism in a van der Waals crystal down to the monolayer limit, *Nature* 546, 270 (2017)
14. C. Gong, L. Li, Z. L. Li, H. W. Ji, A. Stern, Y. Xia, T. Cao, W. Bao, C. Z. Wang, Y. A. Wang, Z. Q. Qiu, R. J. Cava, S. G. Louie, J. Xia, and X. Zhang, Discovery of intrinsic ferromagnetism in two-dimensional van der Waals crystals, *Nature* 546, 265 (2017)
15. Y. Liu, and C. Petrovic, Critical behavior of quasi-two-dimensional semiconducting ferromagnet $Cr_2Ge_2Te_6$, *Phys. Rev. B* 96, 054406 (2017)
16. Y. Liu and C. Petrovic, Three-dimensional magnetic critical behavior in CrI_3, *Phys. Rev. B* 97, 014420 (2018)
17. X. Zhang, T. L. Yu, Q. Y. Xue, M. Lei, and R. Z. Jiao, Critical behavior and magnetocaloric effect in monoclinic Cr_5Te_8, *J. Alloys Compd.* 750, 798 (2018)
18. Y. Zhu, X. H. Kong, T. D. Rhone, and H. Guo, Systematic search for two-dimensional ferromagnetic materials, *Phys. Rev. Mater.* 2, 081001 (2018)
19. X. W. Zhang, B. Wang, Y. L. Guo, Y. H. Zhang, Y. F.

Chen, and J. L. Wang, High Curie temperature and intrinsic ferromagnetic half-metallicity in two-dimensional Cr_3X_4 (X = S, Se, Te) nanosheets, *Nanoscale Horiz.* 4, 859 (2019)
20. L. Z. Zhang, A. L. Zhang, X. D. He, X. W. Ben, Q. L. Xiao, W. L. Lu, F. Chen, Z. J. Feng, S. X. Cao, J. C. Zhang, and J. Y. Ge, Critical behavior and magnetocaloric effect of the quasi-two-dimensional room-temperature ferromagnet Cr_4Te_5, *Phys. Rev. B* 101, 214413 (2020)
21. J.-J. Xian, C. Wang, J.-H. Nie, R. Li, M. Han, J. Lin, W.-H. Zhang, Z.-Y. Liu, Z.-M. Zhang, M.-P. Miao, Y. Yi, S. Wu, X. Chen, J. Han, Z. Xia, W. Ji, and Y.-S. Fu, Spin mapping of intralayer antiferromagnetism and field-induced spin reorientation in monolayer $CrTe_2$, *Nat. Commun.* 13, 257 (2022)
22. P. Gao, X. Li, and J. Yang, Thickness Dependent magnetic transition in few layer 1T phase $CrTe_2$, *J. Phys. Chem. Lett.* 12, 6847 (2021)
23. H. Y. Lv, W. J. Lu, D. F. Shao, Y. Liu, and Y. P. Sun, Strain-controlled switch between ferromagnetism and antiferromagnetism in 1T-CrX_2 (X = Se, Te) monolayers, *Phys. Rev. B* 92, 214419 (2015)
24. X. Yang, X. Zhou, W. Feng, and Y. Yao, Tunable magneto-optical effect, anomalous Hall effect, and anomalous Nernst effect in the two-dimensional room-temperature ferromagnet 1T-$CrTe_2$, *Phys. Rev. B* 103, 024436 (2021)
25. H. X. Li, L. J. Wang, J. S. Chen, T. Yu, L. Zhou, Y. Qiu, H. T. He, F. Ye, T. K. Sou, and G. Wang, Molecular beam epitaxy grown Cr_2Te_3 thin films with tunable Curie temperatures for spintronic devices, *ACS Appl. Nano Mater.* 2, 6809 (2019)
26. Y. Wen, Z. H. Liu, Y. Zhang, C. X. Xia, B. X. Zhai, X. H. Zhang, G. H. Zhai, C. Shen, P. He, R. Q. Cheng, L. Yin, Y. Y. Yao, M. G. Sendeku, Z. X. Wang, X. B. Ye, C. S. Liu, C. Jiang, C. X. Shan, Y. W. Long, and J. He, Tunable room-temperature ferromagnetism in two-dimensional Cr_2Te_3, *Nano Lett.* 20, 3130 (2020)
27. M. Bian, A. N. Kamenskii, M. Han, W. Li, S. Wei, X. Tian, D. B. Eason, F. Sun, K. He, H. Hui, F. Yao, R. Sabirianov, J. P. Bird, C. Yang, J. Miao, J. Lin, S. A. Crooker, Y. Hou, and H. Zeng, Covalent 2D Cr_2Te_3 ferromagnet, *Mater. Res. Lett* 9, 205 (2021)
28. J. Yao, H. Wang, B. Yuan, Z. Hu, C. Wu, and A. Zhao, Ultrathin van der Waals antiferromagnet $CrTe_3$ for fabrication of in-plane $CrTe_3$/$CrTe_2$ monolayer magnetic heterostructures, *Adv. Mater.* 34, 2200236 (2022)
29. R. Li, J.-H. Nie, J.-J. Xian, J.-W. Zhou, Y. Lu, M.-P. Miao, W.-H. Zhang, and Y.-S. Fu, Planar heterojunction of ultrathin $CrTe_3$ and $CrTe_2$ van der Waals magnet, *ACS Nano* 16, 4348 (2022)
30. W. Y. Wang, J. Y. Fan, H. Liu, H. Zheng, C. L. Ma, L. Zhang, Y. B. Sun, C. X. Wang, Y. Zhu, and H. Yang, Fabrication and magnetic-electronic properties of van der Waals Cr_4Te_5 ferromagnetic films, *Crystengcomm* 24, 674 (2022)
31. J. Wang, W. Y. Wang, J. Y. Fan, H. Zheng, H. Liu, C. L. Ma, L. Zhang, W. Tong, L. S. Ling, Y. Zhu, and H. Yang, Epitaxial growth and room-temperature ferromagnetism of quasi-2D layered Cr_4Te_5 thin film, *J. Phys. D: Appl. Phys.* 55, 165001 (2022)
32. Y. Liu, L. J. Wu, X. Tong, J. Li, J. Tao, Y. M. Zhu, and C. Petrovic, Thickness-dependent magnetic order in CrI_3 single crystals, *Sci. Rep.* 9, 13599 (2019)
33. M. E. Fisher, The theory of equilibrium critical phenomena, *Rep. Prog. Phys.* 30, 615 (1967)
34. H. E. Stanley, Introduction to Phase Transitions and Critical Phenomena, Oxford University Press, London and New York, 1971
35. A. Arrott, Criterion for ferromagnetism from observations of magnetic isotherms, *Phys. Rev.* 108, 1394 (1957)
36. B. K. Banerjee, On a generalised approach to first and second order magnetic transitions, *Phys. Lett.* 12, 16 (1964)
37. A. Arrott and J. E. Noakes, Approximate equation of state for nickel near its critical temperature, *Phys. Rev. Lett.* 19, 786 (1967)
38. M. H. Phan, V. Franco, A. Chaturvedi, S. Stefanoski, G. S. Nolas, and H. Srikanth, Origin of the magnetic anomaly and tunneling effect of europium on the ferromagnetic ordering in $Eu_{8-x}Sr_xGa_{16}Ge_{30}$ (x=0, 4) type-I clathrates, *Phys. Rev. B* 84, 054436 (2011)
39. S. Lin, H. Y. Lv, J. C. Lin, Y. A. Huang, L. Zhang, W. H. Song, P. Tong, W. J. Lu, and Y. P. Sun, Critical behavior in the itinerant ferromagnet $AsNCr_3$ with tetragonal-antiperovskite structure, *Phys. Rev. B* 98, 014412 (2018)
40. A. Rahman, M. U. Rehman, D. C. Zhang, M. Zhang, X. Q. Wang, R. C. Dai, Z. P. Wang, X. P. Tao, L. Zhang, and Z. M. Zhang, Critical behavior in the half-metallic Hensler alloy Co_2TiSn, *Phys. Rev. B* 100, 214419 (2019)
41. B. Widom, Degree of the critical isotherm, *J. Chem. Phys.* 41, 1633 (1964)
42. B. Widom, Equation of state in the neighborhood of the critical point, *J. Chem. Phys.* 43, 3898 (1965)
43. J. Y. Fan, L. S. Ling, B. Hong, L. Zhang, L. Pi, and Y. H. Zhang, Critical properties of the perovskite manganite $La_{0.1}Nd_{0.6}Sr_{0.3}MnO_3$, *Phys. Rev. B* 81, 144426 (2010)
44. A. Perumal, V. Srinivas, V. V. Rao, and R. A. Dunlap, Quenched disorder and the critical behavior of a partially frustrated system, *Phys. Rev. Lett.* 91, 137202 (2003)
45. A. K. Pramanik and A. Banerjee, Critical behavior at paramagnetic to ferromagnetic phase transition in $Pr_{0.5}Sr_{0.5}MnO_3$: A bulk magnetization study, *Phys. Rev. B* 79, 214426 (2009)
46. J. Mira, J. Rivas, M. Vazquez, J. M. Garcia-Beneytez, J. Arcas, R. D. Sanchez, and M. A. Senaris-Rodriguez, Critical exponents of the ferromagnetic-paramagnetic phase transition of $La_{1-x}Sr_xCoO_3$ ($0.20 \le x \le 0.30$), *Phys. Rev. B* 59, 123 (1999)
47. L. P. Kadanoff, W. Götze, D. Hamblen, R. Hecht, E. A. S. Lewis, V. V. Palciauskas, M. Rayl, J. Swift, D. Aspnes, and J. Kane, Static phenomena near critical points: Theory and experiment, *Rev. Mod. Phys.* 39, 395 (1967)
48. R. Thaljaoui, M. M. Nofal, and R. M'Nassri, Thermomagnetic properties and critical behaviour studies in the ferromagnetic-Paramagnetic phase transition in $Pr_{0.6}Sr_{0.35}Ag_{0.05}MnO_3$ and $Pr_{0.6}Sr_{0.3}Ag_{0.1}MnO_3$ ceramics, *Chem. Phys.* 547, 111205 (2021)

49. S. F. Fischer, S. N. Kaul, and H. Kronmuller, Critical magnetic properties of disordered polyerystalline $Cr_{75}Fe_{25}$ and $Cr_{70}Fe_{30}$ alloys, *Phys. Rev. B* 65, 064443 (2002)
50. M. E. Fisher, S.-K. Ma, and B. G. Nickel, Critical exponents for long-range interactions, *Phys. Rev. Lett.* 29, 917–920 (1972)
51. X. J. Yang, J. X. Pan, W. Z. Gai, Y. P. Tao, H. Jia, L. M. Cao, and Y. Cao, Three-dimensional critical behavior and anisotropic magnetic entropy change in quasi-two-dimensional $LaCrSb_3$, *Phys. Rev. B* 105, 024419 (2022)
52. B. J. Liu, Y. M. Zou, S. M. Zhou, L. Zhang, Z. Wang, H. X. Li, Z. Qu, and Y. H. Zhang, Critical behavior of the van der Waals bonded high T_C ferromagnet Fe_3GeTe_2, *Sci. Rep.* 7, 6184 (2017)
53. W. Liu, Y. H. Dai, Y. E. Yang, J. Y. Fan, L. Pi, L. Zhang, and Y. H. Zhang, Critical behavior of the single-crystalline van der Waals bonded ferromagnet $Cr_2Ge_2Te_6$, *Phys. Rev. B* 98, 214420 (2018)
54. Z. F. Li, X. Li, B. Ding, H. Li, Y. Yao, X. K. Xi, and W. H. Wang, Magnetic anisotropy and critical behavior of the quaternary van der Waals ferromagnetic material $Cr_{0.96}Ge_{0.17}Si_{0.82}Te_3$, *J. Phys.: Condens. Matter* 33, 425803 (2021)
55. S. Mondal, N. Khan, S. M. Mishra, B. Satpati, and P. Mandal, Critical behavior in the van derWaals itinerant ferromagnet Fe_4GeTe_2, *Phys. Rev. B* 104, 094405 (2021)
56. Y. Liu, and C. Petrovic, Anisotropic magnetocaloric effect and critical behavior in $CrCl_3$, *Phys. Rev. B* 102, 014424 (2020)
57. A. Bedoya-Pinto, J. R. Ji, A. K. Pandeya, P. Gargiani, M. Valvidares, P. Sessi, J. M. Taylor, F. Radu, K. Chang, and S. S. P. Parkin, Intrinsic 2D-XY ferromagnetism in a van der Waals monolayer, *Science* 374, 616 (2021)
58. G. T. Lin, X. Luo, F. C. Chen, J. Yan, J. J. Gao, Y. Sun, W. Tong, P. Tong, W. J. Lu, Z. G. Sheng, W. H. Song, X. B. Zhu, and Y. P. Sun, Critical behavior of two-dimensional intrinsically ferromagnetic semiconductor CrI_3, *Appl. Phys. Lett.* 112, 072405 (2018)
59. A. Taroni, S. T. Bramwell, and P. C. W. Holdsworth, Universal window for two-dimensional critical exponents, *J. Phys.: Condens. Matter* 20, 275233 (2008)
60. T. Moriya and Y. Takahashi, Spin fluctuation theory of itinerant electron ferromagnetism – A unified picture, *J. Phys. Soc. Jpn.* 45, 397 (1978)
61. Y. Takahashi, On the origin of the Curie–Weiss law of the magnetic susceptibility in itinerant electron ferromagnetism, *J. Phys. Soc. Jpn.* 55, 3553 (1986)
62. M. K. Chattopadhyay, P. Arora, and S. B. Roy, Magnetic properties of the field-induced ferromagnetic state in MnSi, *J. Phys.: Condens. Matter* 21, 296003 (2009)
63. M. Imai, C. Michioka, H. Ueda, and K. Yoshimura, Static and dynamical magnetic properties of the itinerant ferromagnet $LaCo_2P_2$, *Phys. Rev. B* 91, 184414 (2015)